# Collective Motion and Pattern Formation in Phase-Synchronizing Active Fluids

Brato Chakrabarti,[1] Michael J. Shelley,[1,2] and Sebastian Fürthauer[1,3,*]

[1]*Center for Computational Biology, Flatiron Institute, New York, New York 10010, USA*
[2]*Courant Institute, New York University, New York, New York 10012, USA*
[3]*Institute of Applied Physics, TU Wien, A-1040 Wien, Austria*

Many active particles, such as swimming micro-organisms or motor proteins, do work on their environment by going though a periodic sequence of shapes. Interactions between particles can lead to synchronization of their duty cycles. Here, we study the collective dynamics of a suspension of active particles coupled through hydrodynamics. We find that at high enough density the system transitions to a state of collective motion by a mechanism that is distinct from other instabilities in active matter systems. Second, we demonstrate that the emergent nonequilibrium states feature stationary chimera patterns in which synchronized and phase-isotropic regions coexist. Third, we show that in confinement, oscillatory flows and robust unidirectional pumping states exist, and can be selected by choice of alignment boundary conditions. These results point toward a new route to collective motion and pattern formation and could guide the design of new active materials.

*Introduction.*—Many microbes, motor-laden cytoskeletal assemblies, and many of their nonliving analogs do work on their surroundings by undergoing a mechano-chemical duty cycle [1,2]. For instance, swimming algae move by cyclical deformations of their flagella and the dipole strength associated with their beat changes sign over the flagellar duty cycle [3]. On timescales longer than the duty cycle, this often results in net cycle-averaged dipolar stresses, which if strong enough, drive instabilities resulting in local ordering and collective motion [4,5]. Here, we concern ourselves with suspensions of immotile active particles whose cycle-averaged force dipole is zero. For these, the above-mentioned route towards self-organization is precluded [6]. However, an alternate route towards collective motion, based on phase synchronization, has been predicted [7–10]. In this Letter, we confirm that suspensions of active particles can indeed spontaneously form collectively moving states by synchronizing their phases, and we characterize the properties of such previously unknown synchronized states. We find that the emergent states are chimeras in which phase ordered and disordered regions coexist. In confinement, synchronization-based self-organization can generate steady unidirectional flows, where active particles self-organize into an active pump or collective oscillations. The transition between these two behaviors is controlled by boundary conditions. Our work reveals and characterizes a previously unconfirmed mode of collective motion for microbial, cytoskeletal, and engineered immotile active particle suspensions.

Most active matter theories are formulated in terms of cycle averaged stresses [4]. However, versions which quantify the progression along an internal duty cycle of an active particle by a phase $\varphi \in [0, 2\pi)$, that modulates the active stress, also exist [7–10]. Intriguingly, linear stability analysis of these theories had suggested that active particles could spontaneously synchronize their phases and form patterned states. By analogy to another much-studied example of phase patterning—the formation of metachronal waves in ciliary arrays [11–17], where ciliary coordination results in large scale fluid flows, it was speculated [7–9] that the phase-patterned states emerging in synchronizing active particles could also drive fluid flows. Prior to this Letter, this had remained speculation, since it was unclear whether results from the ciliary system, in which anchored active elements generate force monopoles on the fluid, would translate to active suspensions, in which suspended active elements generate force dipoles. We resolve this issue by numerically studying the nonequilibrium dynamics of synchronizing active fluids [7]. We find and characterize the flows and patterns in phase-synchronizing active suspensions and show that they emerge via a mechanism that is distinct from the classic instabilities known from phase-isotropic active matter [2,4,18]. We show how to control the emergent states via boundary conditions, and in the Supplemental Material [19] we suggest a toy model of an active oscillator that could guide the design of new active matter systems.

We first delineate a theory for active phase synchronizing suspensions, which extends [7] by including orientational dynamics. Consider a 2D suspension of apolar active particles immersed in a Stokesian fluid. The probability density of particles with phase $\varphi$ at position $\mathbf{x}$ is given by $\psi(\mathbf{x}, \varphi, t)$ and obeys the Smoluchowski equation

$$\partial_t\psi + v_\beta\partial_\beta\psi + \partial_\varphi(\dot{\varphi}\psi) - D\partial_\beta^2\psi = 0, \tag{1}$$

where $D$ is the translational diffusion, $\mathbf{v}(\mathbf{x}) = (u, v)$ is the fluid velocity, and Einstein summation is implied. Each particle is characterized by an additional unit vector $\mathbf{n}$ that describes particle orientation. Here, we only treat sharply aligned 2D nematic states where the nematic tensor is $Q_{\alpha\beta} = n_\alpha n_\beta - \delta_{\alpha\beta}/2$ and particles at location $\mathbf{x}$ point along the local director $\mathbf{n}(\mathbf{x}, t) = [\cos\theta(\mathbf{x}, t), \sin\theta(\mathbf{x}, t)]$.

Following [7] we take the phase-velocity $\dot{\varphi}$ as

$$\dot{\varphi} = \Omega_0 + X(\varphi)Q_{\alpha\beta}E_{\alpha\beta} - d_\varphi\partial_\varphi\ln\psi, \qquad (2)$$

where $E_{\alpha\beta} = (\partial_\alpha v_\beta + \partial_\beta v_\alpha)/2$ is the rate-of-strain tensor and the phase velocity of isolated particles in a quiescent fluid is $\Omega_0$. Here, we have conceptualized the particles as apolar dumbbells that generate stresses by surface deformations. Fluid flows, which can be generated externally or by other particles, will induce additional stresses that can alter this dynamics. The coupling function $X(\varphi)$ encodes this. Since the same applied strain rate $E_{\alpha\beta}$ that helps a particle's extension in its extensile phase will hinder its contraction during its contractile phase, $X(\varphi)$ is phase dependent; see Supplemental Material [19,20]. The last term in Eq. (2) accounts for phase diffusion and $d_\varphi$ is the phase diffusivity.

The surrounding fluid obeys

$$\eta\partial_\beta^2 v_\alpha - \partial_\alpha q + \partial_\beta(\sigma_{\alpha\beta}^{\rm act} + \sigma_{\alpha\beta}^{\rm el}) = 0, \qquad (3)$$

where $\eta$ is the shear viscosity, and the pressure $q$ enforces incompressibility $\partial_\beta v_\beta = 0$. Further, $\sigma_{\alpha\beta}^{\rm act}$ is the active stress that particles exert on the fluid. The elastic stress $\sigma_{\alpha\beta}^{\rm el}$ is generated by alignment interactions between particles. The active stress is given by

$$\sigma_{\alpha\beta}^{\rm act}(\mathbf{x}, t) = Q_{\alpha\beta}\int_0^{2\pi}\psi(\mathbf{x}, \varphi, t)s(\varphi)\dot{\varphi}\,{\rm d}\varphi, \qquad (4)$$

where $s(\varphi)$ is a $2\pi$-periodic function that describes the details of the force production mechanism. The surface stress is proportional to the phase-speed $\dot{\varphi}$, since the active stresses are generated through cyclic surface deformation of the particles. We choose $s(\varphi) = S\cos\varphi$ and thus particles with a constant phase velocity generate no cycle-averaged active stress.

Particle alignment produces an elastic stress $\sigma_{\alpha\beta}^{\rm el}(\mathbf{x}, t) = n_\alpha h_\beta$ on the fluid, where the molecular alignment field $\mathbf{h} = -\delta f^{\rm el}/\delta\mathbf{n}$, and $f^{\rm el}$ is the alignment free-energy density [21]. The evolution of the director field for rodlike bodies [22] obeys

$$\frac{{\rm D}n_\alpha}{{\rm D}t} = \frac{1}{\gamma}h_\alpha - (\partial_\alpha v_\beta)n_\beta, \qquad (5)$$

where ${\rm D}/{\rm D}t = \partial_t + v_\beta\partial_\beta$ is the material derivative, $\gamma$ is the rotational viscosity, and $\partial_\alpha v_\beta$ is the velocity gradient tensor.

Using the single constant Frank elasticity approximation we write $f^{\rm el} = K(\partial_\alpha n_\beta)^2/2 + h_\|(n_\beta n_\beta - 1)/2$, where $h_\|$ is the Lagrange multiplier that guarantees $|\mathbf{n}| = 1$ [21,23]. The interaction of elasticity with activity introduces the Freedericksz length $\ell_{\rm f} = L\sqrt{K/S\Omega_0}$, where $L$ is the system size [24]. In the limit $\ell_f \gg L$, the director field does not deform, and the molecular alignment field $h_\alpha = \gamma n_\beta\partial_\alpha v_\beta$ acts as the Lagrange multiplier that enforces ${\rm D}\mathbf{n}/{\rm D}t = 0$.

To describe synchronization, we introduce the order-parameter fields $Z_n(\mathbf{x}, t) = \int_0^{2\pi}e^{in\varphi}\psi(\mathbf{x}, \varphi, t){\rm d}\varphi$ where $n \in \mathbb{Z}$ i.e. the Fourier coefficients of the distribution function in $\varphi$ [7]. By construction $Z_0 \equiv c(\mathbf{x}, t)$ is the concentration field and $Z_1(\mathbf{x}, t)$ is the complex Kuramoto order field. Synchronized states correspond to $|Z_1| \approx 1$, while $|Z_1| \approx 0$ is associated with phase disorder. The active stress in Eq. (4) can be written as $\sigma_{\alpha\beta}^{\rm act} = \mathcal{M}(\mathbf{x})Q_{\alpha\beta}$ (see Supplemental Material [19]) where

$$\mathcal{M}(\mathbf{x}) = \frac{(\Omega_0 + imd_\varphi)s_m Z_{-m}}{2\pi} + \frac{E_{\mu\nu}Q_{\mu\nu}s_m X_n Z_{-(n+m)}}{4\pi^2}. \qquad (6)$$

Here $s_m$, $X_m$ are the Fourier coefficients of $s(\varphi)$ and $X(\varphi)$, respectively. Using Eq. (1) we obtain

$$\frac{{\rm D}Z_n}{{\rm D}t} - D\partial_\beta^2 Z_n + n^2 d_\varphi Z_n = in\left(\Omega_0 Z_n + E_{\alpha\beta}Q_{\alpha\beta}\frac{X_m Z_{n-m}}{2\pi}\right). \qquad (7)$$

Equations (7) couple all moments $Z_n$; however, if $d_\varphi > 0$ the higher-order moments decay rapidly. Here, we evolve $Z_{1,2,3}$ and approximate $Z_4 \approx Z_2^2/c$. Retaining higher order moments did not alter the results obtained through this closure and limited simulations of the full kinetic model where also consistent. Hence, here we explore the model by evolving Eqs. (3) and (5)–(7). As outlined in [7], the model exhibits hydrodynamic instabilities when the coupling function $X(\varphi)$ is phase-shifted from $s(\varphi)$. For simplicity we use $X(\varphi) = A\cos(\phi - \bar{\phi})$, where $\bar{\phi}$ is the phase shift. Including higher harmonics in $X(\varphi)$, $s(\varphi)$ did not alter the qualitative behavior (see Supplemental Material [19]).

*Linear stability.*—To delineate the role of synchronization, we first seek understanding of the simpler case, where $\dot{n} = 0$, which is relevant if $\ell_{\rm f} \gg L$. For $d_\varphi > 0$ the phase-disordered state, with $Z_0 = c_0$, $\mathbf{v} = \mathbf{0}$, and $Z_n = 0$, is the sole fixed point of this problem. For periodic boundary conditions, consistent with [7], the phase-disordered state has a long wavelength Hopf bifurcation (see Supplemental Material [19]). The most unstable wave vector is set by the direction of largest shear. Because of incompressibility, this is at an angle of 45° above or below the vector $\mathbf{n}$; see Fig. 1(a). We next analyze the stability inside a channel of height $H$ with no slip applied at $y = \pm H/2$. We set $d_\varphi\partial_y Z_n|_{y=\pm H/2} = 0$ that enforces impermeable boundaries.
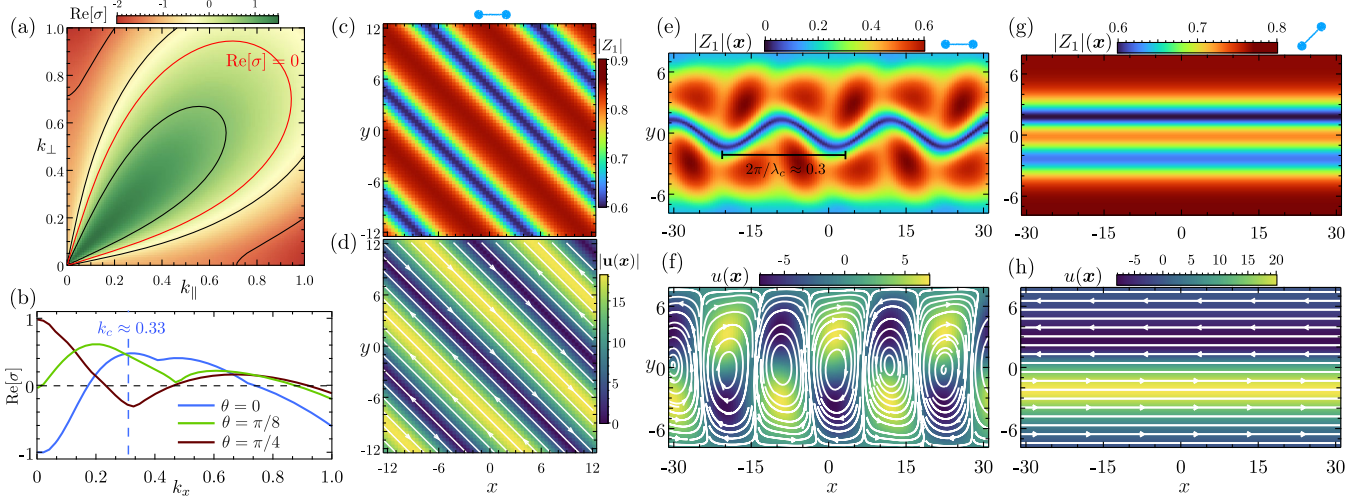
FIG. 1. (a) The real part of the growth rate $\sigma$ as a function of wave numbers $\{k_\parallel, k_\perp\}$ in a periodic box, where $k_\parallel$ and $k_\perp$ are wave vectors parallel and normal to the fixed particle orientation **n**, respectively. The unstable region is within the red curve. (b) Growth rate in a channel, computed from the linear stability as a function of the wave number $k_x$ for different particle alignments. The dominant wave number $k_c$ for $\theta = 0$ is indicated. A snapshot of the Kuramoto order parameter $|Z_1(\mathbf{x})|$ (top) and instantaneous streamlines (bottom) from the emergent travelling wave state is shown for a periodic box (c),(d) and in a channel for $\theta = 0$ (e),(f), and $\theta = \pi/4$ (g),(h). Parameters: $\eta = 2$, $\gamma = 1$, $c_0 = \omega_0 = 8$, $X(\varphi) = \cos\varphi + 2\sin\varphi$. Channel height, $H = 5\pi$. Illustration of the active particles indicates their orientation.

With the Ansatz $\{\mathbf{v}, Z_1\} \to \varepsilon\{\mathbf{v}(y), Z_1(y)\}\exp(ik_x + \sigma t)$, where $\varepsilon \ll 1$, the growth rate $\sigma$ can be computed numerically; see Fig. 1(d). Like in the periodic domain, the phase-disordered state is linearly unstable. Here, the wave number of the fastest growth $k_c$ is set by the channel height $H$ and the particles' orientation. We next study the dynamics of the system beyond the linear regime using spectral simulations [25].

*Nonlinear dynamics.*—Figures 1(c)–1(f) show the spatial structure of the phase-order parameter and the associated fluid flows for fixed $\mathbf{n} = \hat{\mathbf{e}}_x$ inside a periodic box and a channel, respectively. In periodic domains, the Kuramoto order parameter $|Z_1|(\mathbf{x})$ and consequently the velocity $\mathbf{v}(\mathbf{x})$ settle into a striped travelling wave (see movie S1 in the Supplemental Material [19]). The patterns are at the scale of the computational box, consistent with having emerged from a long-wavelength instability [Figs. 1(c) and 1(d)]. Further, again consistent with the stability analysis, the

modulated stripes are orthogonal to the wave vector of maximum growth (45°) and the wave speed is parallel to it.

In channels, with $\mathbf{n} = \hat{\mathbf{e}}_x$, Eq. (2) at the boundaries reduces to $\dot{\varphi} = \Omega_0 - d_\varphi \partial_\varphi \ln\psi$. This predicts that $|Z_1| \approx 0$ near the wall, which is indeed seen from the simulations on Fig. 1(e). Consequently, the instability produces a traveling wave along $\hat{\mathbf{e}}_x$ with a modulated pattern in $|Z_1|$, which has a width of $\lambda_c \approx 2\pi/k_c$ consistent with linear stability. Figure 1(e) further shows that the emergent state is a chimera state [26] with the coexistence of the phase-disordered ($|Z_1| \approx 0$) and phase-synchronized ($|Z_1| \simeq 1$) regions. The associated fluid flows show the formation of vortical structures between them (see Fig. 1(f) and movie S2 in the Supplemental Material [19]). Our results demonstrate that even when the system size is below the Freedericksz length, phase synchronization can provide a novel route toward instabilities. The associated self-organized flows seen in Fig. 1 are distinct from those seen in classical orientation instabilities [2,4,18,24,27], which all depend on nonuniform alignment throughout the domain.

We next characterize emergent states in the channel. For this we probe the zero wave number limit associated with transport. We find from Eq. (3) that $\langle u \rangle = 0$ when $\mathbf{n} = \hat{\mathbf{e}}_x$ or $\hat{\mathbf{e}}_y$, where $\langle \cdot \rangle$ denotes the spatial average of any field variable. As we increase $\theta$ starting from $\theta = 0$, the system instead settles into a pumping state. For these, $|Z_1|$ evolves into a travelling wave along the channel length accompanied by an emergence of a steady flow along $\hat{\mathbf{e}}_x$. The associated fluid flow is characterized by tilted vortices and fluid jets (see movie S3 in the Supplemental Material [19]). The steady flux $\langle u \rangle$ from the final state increases with
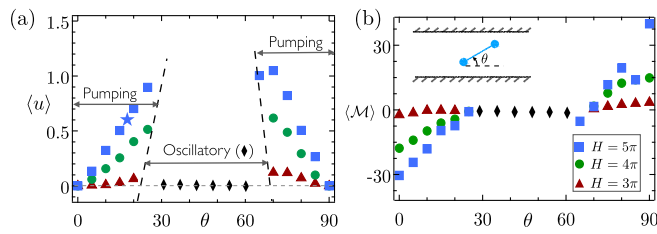


FIG. 2. (a) Phase diagram of the two emergent states: spontaneous pumping and oscillations. (b) Mean amplitude of the active stress $\langle \mathcal{M} \rangle$ as a function of $\theta$ for varying channel height $H$. The asterisk on (a) indicates the state shown in Fig. 3.
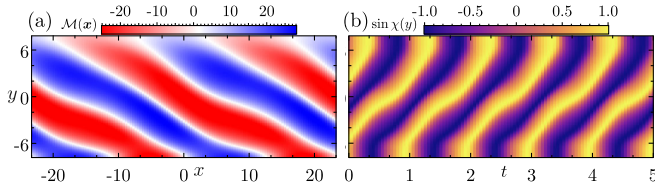
FIG. 3. (a) Variation of $\mathcal{M}(\mathbf{x})$ in the channel demonstrates that through synchronization the suspension behaves as an extensile (or contractile) fluid. Also shown is the direction of pumping results from the spatial distribution of the stress. (b) Variation of the phase along the channel width as a function of time illustrates the existence of metachronal phase waves. Parameters: $H = 5\pi$, $L = 3H$, $\theta = \pi/8$, $\gamma = 1$, $\eta = 2$, $\omega_0 = 8$, $d_\varphi = 1$, $D = 1$, $X(\varphi) = \cos\varphi + 2\sin\varphi$.

the channel height $H$ and the particle orientation $\theta$; see Fig. 2(a). By symmetry, either pumping direction is equally likely, and initial conditions set the final direction.

To better understand the mechanism of the pumping, we next study $\mathcal{M}(\mathbf{x})$ from the final state, which is the amplitude of the active stress $\sigma_{\alpha\beta}^{\mathrm{act}} = \mathcal{M}\mathcal{Q}_{\alpha\beta}$. We find that $\langle\mathcal{M}(\mathbf{x})\rangle$ is identical for both left and right pumping states with the same $\theta$ and has a nonzero mean throughout the pumping regime; see Fig. 2(b). This means that the system has settled into a state of mean extensile (or contractile) active stress [see Fig. 2(b)] through phase synchronization even though the constituent active particles do not have any mean dipole. The direction of pumping is dictated by the difference of the values of $\mathcal{M}(\mathbf{x})$ at the boundaries. Simply put, the axial force per unit depth exerted by the active stresses on the walls is

$\int d\mathbf{x}[(\mathcal{M}\mathcal{Q}_{xy})|_{y=H/2} - (\mathcal{M}\mathcal{Q}_{xy})|_{y=-H/2}]$. This is nonzero if the phase ordering is different for the particles on opposite walls and $\theta \neq 0, \pi/2$. In this case, the particles on average act more pusher-like in one wall and puller-like near the other. This mechanism is further illustrated by the phase kymographs shown in Fig. 3(b), where we plot the phase $\chi(\mathbf{x}, t) = \arg[Z_1(\mathbf{x}, t)]$ at a given $x$ as a function of time. Figure 3(b) indicates the existence of metachronal phase waves associated with pumping. Thus, our simulations demonstrate (i) the spontaneous emergence of coherent fluid transport by phase synchronization, and (ii) the spontaneous emergence of polar pumping states from a globally aligned suspension.

Note that this pumping state loses stability as $\theta$ approaches $\pi/4$, giving rise to oscillatory states instead. Numerical evidence in Fig. 2(b) suggests that the loss of stability of the pumping states is associated with the suspension transitioning from being extensile to contractile with $\langle\mathcal{M}\rangle \approx 0$. Figures 1(g) and 1(h) show an oscillatory state for $\theta = \pi/4$ (see movie S3 in the Supplemental Material [19]). The snapshots highlight that the phase modulations span the entire channel width, consistent with the linear stability; see Fig. 1(b). The Kuramoto order parameter and the associated velocity field organize into travelling waves moving from wall to wall and resulting in the formation of fluid jets along the channel length whose direction oscillates periodically over time. Importantly, since these waves do not break translational symmetry in the $\hat{\mathbf{e}}_x$ direction when averaged over a period, they generate no mean flow. As can be seen from Fig. 2(a), such system-wide oscillatory states exist around a range of orientation around $\theta = \pi/4$. At high enough $\theta$, the pumping state reemerges.
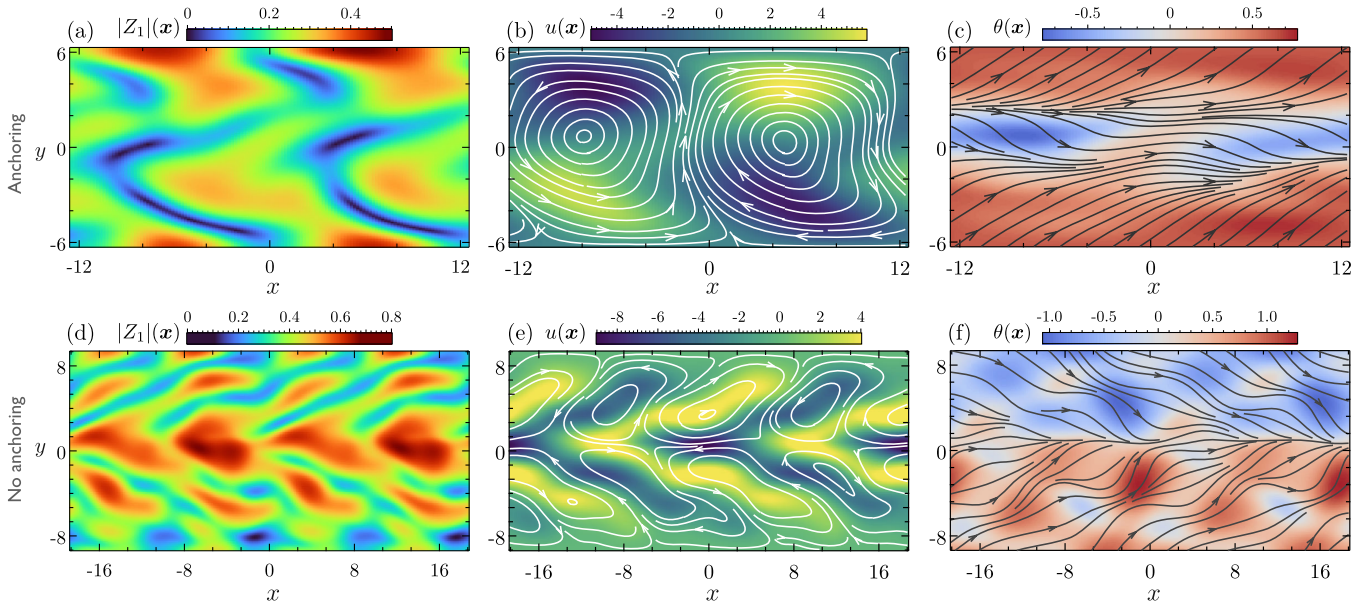


FIG. 4. Snapshots of various field variables for two different boundary conditions of particles. (a),(d) The Kuramoto order parameter from the final state. (b),(e) Associated snapshot of the velocity field and the streamlines highlight the formation of vortical structures and fluid jets. (c),(f) $\theta(\mathbf{x})$ showcases the variation in the orientation and the associated director field. Prameters: (top row) $H = 4\pi$, $L = 8\pi$, $\theta|_{y=\pm H/2} = \pi/5$ and (bottom row) $H = 6\pi$, $L = 12\pi$, $\partial_y\theta|_{y=\pm H/2} = 0$.

We next asked how the system self-organizes if the director **n** evolves according to Eq. (5) ($\dot{n} \neq 0$). In Fig. 4 we show simulation results in a channel for two boundary conditions: (i) anchoring with $\theta|_{y=\pm H/2} = \theta_0$ and (ii) no anchoring with $\partial_y \theta|_{y=\pm H/2} = 0$. When the particles are anchored at the boundary, we find that for small $\theta_0$ the system settles down to a state of coherent mean transport. Similar to the case of $\dot{n} = 0$, we find that the suspension transitions to oscillatory flows upon increasing $\theta_0$. In absence of anchoring, we observe that for all the explored channel heights, the active fluid always settles into a travelling wave state or a periodic orbit (see movie S5 in the Supplemental Material [19]). This emergent state is characterized by coherent fluid pumping and propagating metachronal phase waves. Figure 4(f) shows the director field that develops in the channel. Both the orientations and the phases of the particles, on average, remain mirror symmetric around $y = 0$. The average particle orientations on either side of the channel centerline are accompanied by left- and right-going metachronal phase waves that aid fluid pumping resulting in coherent transport. Importantly, these results demonstrate that boundary conditions control the emergent states.

We finally probe whether the emergent fluid flows in the $\dot{n} \neq 0$ system result from the dynamics of particle orientation or synchronization. For this, we study the dynamics of a $\dot{n} \neq 0$ nematic fluid driven by an active stress $\sigma_{\alpha\beta}^{\mathrm{act}} = \zeta_0 \sin(2\pi f_c t) n_\alpha n_\beta$. Here, $f_c$ is the frequency of the forcing and is obtained from the power spectral density of the steady-state active shear stress $\sigma_{xy}^{\mathrm{act}}$ of the active fluid and $\zeta_0$ is chosen to be the maximum of the measured $\sigma_{xy}^{\mathrm{act}}$; see Supplemental Material [19]. This active forcing mimics the stresses generated by oscillating dipoles that are free to align but unable to synchronize. We find that this stress does not drive any alignment instability and the fluid velocity decays after a short transient demonstrating that synchronization drives the flows shown in Fig. 4.

To conclude, we have characterized a new route towards self-organized flows in active suspensions. Rather than stemming from the cycle averaged stress dipoles, which active particles exert on a timescale much larger than their duty cycles, this second route stems from synchronization between particles, and exists even if the cycle averaged stress generated by isolated constituent particles is zero. The emergent travelling waves are chimeras [28] with regions of high and low synchrony. In confinement, collective states that drive coherent large scale transport of fluid and collective states that drive collective oscillations exist. The type of emergent state can be chosen by controlling boundary conditions. In the Supplemental Material [19], we give a description of how such a system might be constructed.

Coupled mechano-chemical oscillators are involved in important processes like somitogenesis [29] and have also been invoked to explain bacterial pattern formation [30]. However, in these examples, the coupling between oscillators happen through chemical degrees of freedom [31]. The mechanism we uncovered here is based on hydrodynamic interactions and provides a novel route to phase patterning in mechanochemical oscillators that is clearly distinct from [10,29,30]. It is also distinct from other mechanisms that have been invoked to explain biological patterns such as the classical Turing instability [32–34] and its generalizations to phase-insensitive active matter [33,34]. Overall, synchronization provides a new route towards emergent dynamics in active materials. This finding will inform our understanding of collectively moving microbes and motorized cytoskeletal structures, and potentially facilitate the engineering of active materials [31] that can act as micropumps.

---

*fuerthauer@iap.tuwien.ac.at

[1] D. Saintillan and M. J. Shelley, C.R. Phys. **14**, 497 (2013).

[2] M. C. Marchetti, J.-F. Joanny, S. Ramaswamy, T. B. Liverpool, J. Prost, M. Rao, and R. A. Simha, Rev. Mod. Phys. **85**, 1143 (2013).

[3] J. S. Guasto, K. A. Johnson, and J. P. Gollub, Phys. Rev. Lett. **105**, 168102 (2010).

[4] D. Saintillan and M. J. Shelley, Phys. Rev. Lett. **100**, 178103 (2008).

[5] A. Baskaran and M. C. Marchetti, Proc. Natl. Acad. Sci. U.S.A. **106**, 15567 (2009).

[6] T. Brotto, D. Bartolo, and D. Saintillan, J. Nonlinear Sci. **25**, 1125 (2015).

[7] S. Fürthauer and S. Ramaswamy, Phys. Rev. Lett. **111**, 238102 (2013).

[8] M. Leoni and T. B. Liverpool, Phys. Rev. Lett. **112**, 148104 (2014).

[9] T. Banerjee and A. Basu, Phys. Rev. E **96**, 022201 (2017).

[10] K. P. O'Keeffe, H. Hong, and S. H. Strogatz, Nat. Commun. **8**, 1 (2017).

[11] N. Uchida and R. Golestanian, Phys. Rev. Lett. **104**, 178103 (2010).

[12] N. Uchida and R. Golestanian, Phys. Rev. Lett. **106**, 058104 (2011).

[13] J. Elgeti and G. Gompper, Proc. Natl. Acad. Sci. U.S.A. **110**, 4470 (2013).

[14] D. R. Brumley, M. Polin, T. J. Pedley, and R. E. Goldstein, J. R. Soc. Interface **12**, 20141358 (2015).

[15] F. Meng, R. R. Bennett, N. Uchida, and R. Golestanian, Proc. Natl. Acad. Sci. U.S.A. **118**, e2102828118 (2021).

[16] B. Chakrabarti, S. Fürthauer, and M. J. Shelley, Proc. Natl. Acad. Sci. U.S.A. **119**, e2113539119 (2022).

[17] A. Kanale, F. Ling, H. Guo, S. Fuerthauer, and E. Kanso, Proc. Natl. Acad. Sci. U.S.A. **119**, e2214413119 (2022).

[18] R. A. Simha and S. Ramaswamy, Phys. Rev. Lett. **89**, 058101 (2002).

[19] See Supplemental Material at http://link.aps.org/supplemental/10.1103/PhysRevLett.130.128202 for microscopic details of the model, stability analysis and numerical methods, details on the design of new active material, and movies.

[20] G. Batchelor, J. Fluid Mech. **44**, 419 (1970).

[21] P.-G. De Gennes and J. Prost, *The Physics of Liquid Crystals* (Oxford University Press, Oxford, 1993), Vol. 83.

[22] F. Jülicher, S. W. Grill, and G. Salbreux, Rep. Prog. Phys. **81**, 076601 (2018).

[23] R. Ramaswamy, G. Bourantas, F. Jülicher, and I. F. Sbalzarini, J. Comput. Phys. **291**, 334 (2015).

[24] R. Alert, J.-F. Joanny, and J. Casademunt, Nat. Phys. **16**, 682 (2020).

[25] K. J. Burns, G. M. Vasil, J. S. Oishi, D. Lecoanet, and B. P. Brown, Phys. Rev. Res. **2**, 023068 (2020).

[26] D. M. Abrams and S. H. Strogatz, Phys. Rev. Lett. **93**, 174102 (2004).

[27] R. Alert, J. Casademunt, and J.-F. Joanny, Annu. Rev. Condens. Matter Phys. **13** (2021).

[28] E. A. Martens, S. Thutupalli, A. Fourrière, and O. Hallatschek, Proc. Natl. Acad. Sci. U.S.A. **110**, 10563 (2013).

[29] K. Uriu, R. Bhavna, A. C. Oates, and L. G. Morelli, Biol. Open **6**, 1235 (2017).

[30] O. A. Igoshin, A. Mogilner, R. D. Welch, D. Kaiser, and G. Oster, Proc. Natl. Acad. Sci. U.S.A. **98**, 14913 (2001).

[31] S. Thutupalli, R. Seemann, and S. Herminghaus, New J. Phys. **13**, 073021 (2011).

[32] A. M. Turing, Bull. Math. Biol. **52**, 153 (1990).

[33] J. Howard, S. W. Grill, and J. S. Bois, Nat. Rev. Mol. Cell Biol. **12**, 392 (2011).

[34] J. S. Bois, F. Jülicher, and S. W. Grill, Phys. Rev. Lett. **106**, 028103 (2011).